

Probing spin-isospin excitations in proton-rich nuclei via the $^{11}\text{C}(p, n)^{11}\text{N}$ reaction

J. Schmitt ^{1,2,3,*} G. B. King ⁴ R. G. T. Zegers ^{1,2,3,†} Y. Ayyad ^{1,5} D. Bazin ^{1,2} B. A. Brown ^{1,2,3} A. Carls ^{1,2,3} J. Chen,¹
A. Davis,^{1,2,3} M. DeNudt,^{1,2,3} J. Droste ^{1,2,3} B. Gao ^{1,2,6} C. Hultquist,^{1,2,3} H. Iwasaki ^{1,2,3} S. Noji ^{1,2} S. Pastore,⁴
J. Pereira,^{1,2} M. Piarulli ⁴ H. Sakai ⁷ A. Stolz,¹ R. Titus,^{1,2,3} R. B. Wiringa ⁸ and J. C. Zamora ^{1,9}

¹Facility for Rare Isotope Beams, Michigan State University, East Lansing, Michigan 48824, USA

²Department of Physics and Astronomy, Michigan State University, East Lansing, Michigan 48824, USA

³Joint Institute for Nuclear Astrophysics, Michigan State University, East Lansing, Michigan 48824, USA

⁴Department of Physics, Washington University, St. Louis, Missouri 63130, USA

⁵IGFAE, Universidade de Santiago de Compostela, E-15782, Santiago de Compostela, Spain

⁶Institute of Modern Physics, Chinese Academy of Sciences, Lanzhou 730000, China

⁷Department of Physics, The University of Tokyo, Bunkyo, Tokyo 113-0033, Japan

⁸Physics Division, Argonne National Laboratory, Argonne, Illinois 60439, USA

⁹Instituto de Física, Universidade de São Paulo, São Paulo 05508-090, Brazil



(Received 31 July 2022; accepted 20 October 2022; published 23 November 2022)

Tracking the evolution of nuclear properties away from stability serves as a valuable test for nuclear models. In the present work, the (p, n) charge-exchange reaction was used to test the extraction of β^- Gamow-Teller transition strengths, $B(\text{GT})$, from proton-rich unstable isotopes, and the resulting $B(\text{GT})$ values were compared to shell-model and *ab initio* calculations. The $^{11}\text{C}(p, n)^{11}\text{N}$ reaction was measured in inverse kinematics at 95 MeV/u at the National Superconducting Cyclotron Laboratory. The $B(\text{GT})$ values to the $\frac{1}{2}^-$ state at 0.73 MeV and the $\frac{3}{2}^-$ state at 2.86 MeV in ^{11}N were determined to be $0.18(1)^{\text{stat}}(3)^{\text{sys}}$ and $0.18(1)^{\text{stat}}(4)^{\text{sys}}$, respectively. These results are consistent with shell-model calculations using the *wbp* interaction after introducing a phenomenological quenching factor and with *ab initio* variational Monte Carlo calculations using the $NV2 + 3Ia^*$ NN and $3N$ interactions without any scaling. Additionally, this result is consistent with the $B(\text{GT})$ values extracted from mirror $^{11}\text{B}(n, p)$ and $^{11}\text{B}(t, ^3\text{He})$ reactions. This experiment demonstrates the feasibility of using the (p, n) probe in inverse kinematics to extract $B(\text{GT})$ from proton-rich nuclei, although improved background suppression will be important in future experiments.

DOI: [10.1103/PhysRevC.106.054323](https://doi.org/10.1103/PhysRevC.106.054323)

I. INTRODUCTION

The properties of nuclei evolve as one moves from the valley of stability to the driplines. Furthermore, nuclei that are located near, at, and beyond the driplines can exhibit new phenomena, such as halos [1–3] and novel decay modes [4,5]. Due to their novel properties, exotic nuclei provide fertile testing grounds for theoretical models. A famous example is the case of ^{11}Be , whose ground state exhibits a halo structure and demonstrates parity inversion [6,7]. Its isospin-symmetric partner ^{11}N also exhibits parity inversion for its ground state, but unlike ^{11}Be is unbound. An interesting question is whether there is a significant difference between the properties of the wave functions of the low-lying states of these two nuclei driven by the large neutron (^{11}Be) and proton (^{11}N) excesses to the extent that they impact the Gamow-Teller (GT) transition strength, or $B(\text{GT})$, distributions.

The purpose of this work is to measure the $B(\text{GT})$ values for $^{11}\text{C}[\text{g.s.}] \rightarrow ^{11}\text{N}^*$ transitions and compare the results to previously measured $B(\text{GT})$ values from mirror $^{11}\text{B}[\text{g.s.}] \rightarrow$

$^{11}\text{Be}^*$ transitions. The wave functions of both $^{11}\text{B}[\text{g.s.}]$ and $^{11}\text{C}[\text{g.s.}]$ are well known to be p -shell configurations, so a measure of $B(\text{GT})$ would provide information about the p -shell content of ^{11}Be and ^{11}N wave functions. The experimental results are interpreted and compared with shell-model and *ab initio* variational Monte Carlo (VMC) calculations.

$B(\text{GT})$ is directly measured via β decay. However, β decay is limited by the decay Q value, and high-lying excited states (and nuclei that do not β -decay, as in this work) cannot be studied. Charge-exchange (CE) reactions connect the same initial and final states as in β decay, but are not limited by a decay Q value, therefore providing access to states otherwise inaccessible to β decay. $B(\text{GT})$ values can be extracted from the CE cross section via a well-established proportionality relationship with the CE differential cross sections at small momentum transfer ($q \approx 0$) [8]. For example, Meharchand *et al.* [9] extracted $B(\text{GT})$ from the $^{12}\text{B}(^7\text{Li}, ^7\text{Be})^{12}\text{Be}[0_{1,2}^+]$ reaction and used the results to determine the p -shell components of the $0_{1,2}^+$ states. The experimental extraction of the strength does not depend on model assumptions, so this method provides a valuable benchmark to test nuclear models.

$B(\text{GT})$ has already been extracted for $^{11}\text{B}[\text{g.s.}] \rightarrow ^{11}\text{Be}^*$ transitions from $^{11}\text{B}(n, p)$ -type reactions, including $^{11}\text{B}(n, p)$

*schmittj@nscl.msu.edu

†zegers@nscl.msu.edu

[10], $^{11}\text{B}(d, ^2\text{He})$ [11], and $^{11}\text{B}(t, ^3\text{He})$ [12]. However, no data are available for $^{11}\text{C}[\text{g.s.}] \rightarrow ^{11}\text{N}^*$ GT transitions as ^{11}C itself is unstable. The energies and widths of the low-lying states in ^{11}N have previously been studied in multinucleon transfer experiments [13–18] and resonant elastic scattering experiments [19–22]. The previously cited works generally agree from spectroscopic-factor analyses and mirror-symmetry arguments that the first $\frac{1}{2}^-$ state in ^{11}N is a single-particle state with a $^{10}\text{C} \otimes \pi(p_{1/2})$ structure. Reference [20] suggests that the first $\frac{3}{2}^-$ state has a strong coupling to a $^{10}\text{C}[2_1^+]$ core. Reference [18] suggests that this state decays by proton emission to both the ground state and 2_1^+ first excited state of ^{10}C , supporting the hypothesis that the state has a core-excitation component. The p -shell contents of ^{11}N states can be probed more directly by measuring the $B(\text{GT})$ values from the ground state of ^{11}C , which has a p -shell configuration. The measured $B(\text{GT})$ values can then be compared to $B(\text{GT})$ values of isospin-symmetric transitions between ^{11}Be and ^{11}B .

Several CE probes have been developed for the extraction of GT transition strengths. The (p, n) CE reaction at intermediate beam energies ($\gtrsim 100$ MeV/u) is the simplest of these probes and has been used extensively to study stable nuclei [8,23], and in the past 2–3 decades, experimental techniques using the (p, n) reaction in inverse kinematics have been developed to use with rare-isotope beams, see, e.g., Refs. [24–33]. Techniques to reconstruct the reaction from the low-energy recoil neutron using the missing-mass method have been developed in the last decade, see, e.g., Refs. [34–40]. These experiments, however, have been focused on neutron-rich unstable nuclei.

The (p, n) reaction on a proton-rich nucleus decreases the isospin projection T_z by one unit, producing a proton-rich nucleus farther from stability than the target nucleus. This makes proton-rich nuclei, especially relatively light systems, more difficult to study because GT transition strength is partially Pauli blocked in the $\beta^-/(p, n)$ direction. This blocking reduces the yield for charge-exchange reactions relative to other reaction channels that contribute to the background. In addition, for nuclei produced at or beyond the dripline, multiple decay channels are open, which results in final states that can also be populated through other reactions and further contribute to the background.

At the same time, (p, n) experiments on proton-rich systems provide access to unbound nuclei beyond the proton dripline, offering unique opportunities to study nuclear structure. Ultimately, the goal is to study ^{100}Sn , the heaviest known $N = Z$ doubly magic bound nucleus. The $B(\text{GT})$ of its β^+ decay to ^{100}In is the largest known $B(\text{GT}^+)$ [41], suggesting a robust shell closure at $N = Z = 50$. A $^{100}\text{Sn}(p, n)$ experiment could extract $B(\text{GT})$ in the β^- direction to the unbound ^{100}Sb , which would be a valuable test of isospin symmetry. However, measuring (p, n) on such a heavy, proton-rich nucleus is not yet feasible because of the relatively low beam intensities that can presently be obtained. Nevertheless, it is important to develop the techniques to perform such an experiment, while obtaining unique information about lighter proton-rich nuclei at or beyond the dripline.

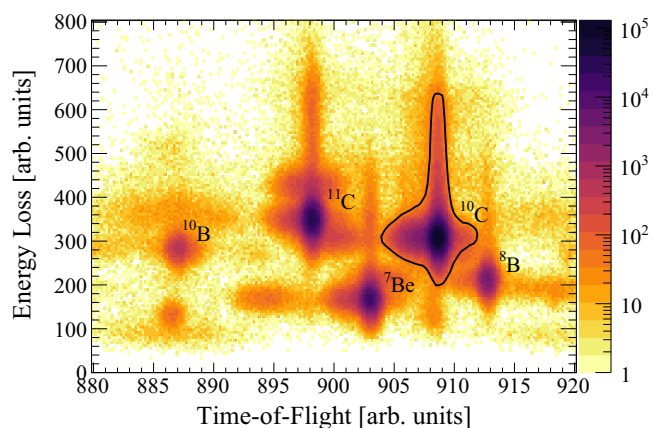


FIG. 1. Particle identification spectrum for the ^{11}C beam. The ^{10}C events are indicated by the black solid outline.

II. EXPERIMENT

The experiment took place at the Coupled Cyclotron Facility (CCF) at the National Superconducting Cyclotron Laboratory (NSCL). A primary beam of ^{16}O with a rate of about 125 pA was created by the Superconducting Source for Ions (SuSI) [42] and accelerated to 150 MeV/u by the K500 and K1200 cyclotrons [43]. The primary beam impinged on a 1175-mg/cm²-thick Be production target, creating a secondary beam via projectile fragmentation. The secondary beam was purified by the A1900 fragment separator [44] with a 1600-mg/cm²-thick Al wedge and 0.5% momentum acceptance. The resulting cocktail beam contained ^{11}C at 95 MeV/u (78%) and ^{12}N at 108 MeV/u (14%), plus a small amount of ^{10}B (7%) and ^{13}O (<1%). The beam particles were identified on an event-by-event basis by using the time-of-flight to the S800 spectrograph object [45]. The effective beam rate was measured by a diamond detector [46] at the S800 spectrograph object to be on average 3.7 MHz with an uncertainty of 8%.

The secondary beam impinged on the Ursinus liquid hydrogen target that was also used in earlier (p, n) experiments [34,35]. The target was placed 65 cm upstream from the pivot point of the S800. The target diameter was 35 mm, and the liquid hydrogen was contained by a 125- μm -thick kapton foil on either side. The hydrogen areal thickness was 50.9(2) mg/cm².

The reaction product of interest, ^{11}N , is unbound and immediately decays to $^{10}\text{C} + p$ or $2\alpha + 3p$. Therefore measurements were taken using two magnetic-rigidity settings in the S800, one for ^{10}C and another for α particles. The S800 focal-plane detectors consisted of two cathode-readout drift chambers (CRDCs)—one exactly at the spectrograph focal plane and the other 1.061 m downstream—that measured the position and angle of heavy residual nucleus, then an ionization chamber that measured the energy loss, and then a plastic scintillator that measured the time. The heavy residual nucleus was identified on an event-by-event basis by its energy loss in the ionization chamber and its time of flight from the S800 object detector to the S800 focal-plane scintillator. The particle identification plot for the ^{10}C magnetic-rigidity setting is shown in Fig. 1. The tails at high energy loss in the

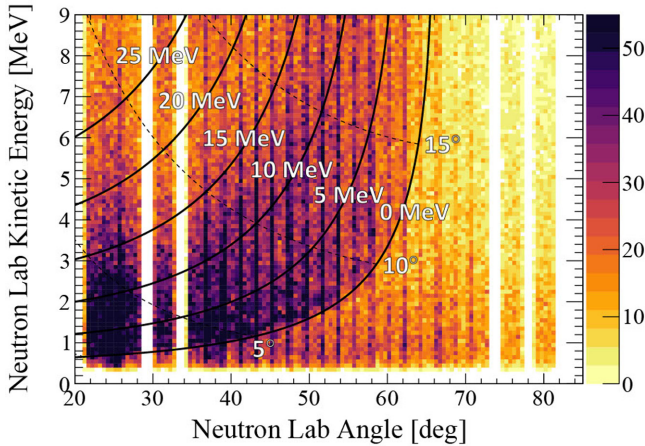


FIG. 2. Neutron laboratory energy vs. laboratory angle measured by LENDA, before background subtraction. The LENDA bars located at the most backward angles beyond the kinematic lines were used to create the background model. Due to space limitations in the laboratory, there are gaps in the LENDA acceptance at 29.2° , 33.5° , 73.8° , and 78.0° .

ionization chamber are from pileup and are counted as good events.

The recoil neutrons from the (p, n) reaction were detected by the Low Energy Neutron Detector Array (LENDAs) [47,48]. LENDA is an array of 24 BC-408 plastic scintillators designed to measure the neutron time of flight for (p, n) reactions in inverse kinematics with rare-isotope beams. The detectors were placed 1 m from the center of the target. Each detector is 30 cm tall ($\Delta\phi = \pm 8.5^\circ$), 4.5 cm wide ($\Delta\theta = \pm 2.6^\circ$), and 2.5 cm deep. The LENDA array covered laboratory angles from 21° to 81° . The neutron energy was calculated from the neutron time-of-flight, where the S800 focal-plane scintillator provided the reference time. The timing resolution was determined from the width of the γ flash to be ≈ 0.9 ns [full width at half-maximum (FWHM)].

III. ANALYSIS

The reaction kinematics were reconstructed using the missing mass method, i.e., the neutron laboratory angle and kinetic energy (shown in Fig. 2) were used to calculate the center-of-mass scattering angle and ^{11}N excitation energy (shown in Fig. 3). There are many events in the negative-excitation-energy region, indicating a significant background component. The background subtraction is explained in this section. Additionally, the vertical artifacts in the data are a result of LENDA bars overlapping or gaps between them. The neutron detection efficiency corrections, including the geometric coverage of the LENDA bars, are also described in this section.

As a consequence of the finite angular resolution of the LENDA bars and the kinematic relationship between the laboratory angle and excitation energy, the excitation energy resolution ranged from 0.9 MeV (FWHM) at forward center-of-mass scattering angles up to 2.0 MeV (FWHM) at the largest scattering angles. Events with hits recorded in more

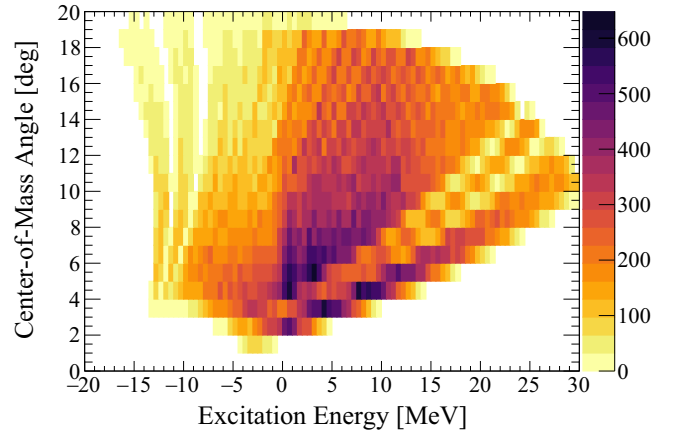


FIG. 3. Center-of-mass scattering angle vs. ^{11}N excitation energy reconstructed via a missing mass calculation, before background subtraction.

than one LENDA bar were discarded. Events with LENDA light output below 65 keVee or above the maximum L_{max} , given in Ref. [48] as a function of neutron kinetic energy, were also discarded. The uncertainty in this maximum from the light-output calibration was propagated to the systematic uncertainty in the final result.

A. Background subtraction

There were three contributions to the background in this experiment: reactions in the kapton foil, random coincidences, and non-CE reactions. Background from carbon in the kapton foils in the target was measured by sending the beam through the empty target cell, and it was negligible. The hydrogen in the foil was included in the effective target-thickness calculation.

Background from random coincidences was modeled from events at unphysically long times of flight. The light-output threshold of 65 keVee removed all neutrons with kinetic energy less than 0.37 MeV, equivalent to times-of-flight greater than 119 ns for a 1 m flight path. Therefore all events with time of flight > 119 ns were random coincidences. The random-coincidence background model was created from a time-of-flight window starting at 130 ns with a width equal to the radiofrequency time, about 42 ns. The events in this window were copied to earlier times to create the random-coincidence background model.

The source of the remaining background was primarily neutron knockout from ^{11}C . The knocked-out neutrons either scattered (indirectly) into LENDA or generated γ rays that hit LENDA but arrived at a time inconsistent with the direct flight path from the target to the detectors. This background was modeled using LENDA bars at angles $> 66^\circ$, the largest angle allowed by the CE reaction kinematics. The resulting background model shape is shown in Fig. 4. The model has a smooth dependence on neutron energy, so the background model shape was copied to each LENDA bar and scaled such that the total counts below $E_x = 0$ MeV would be equal to zero. The statistical uncertainties in the background model were propagated to the statistical error in the final result, and

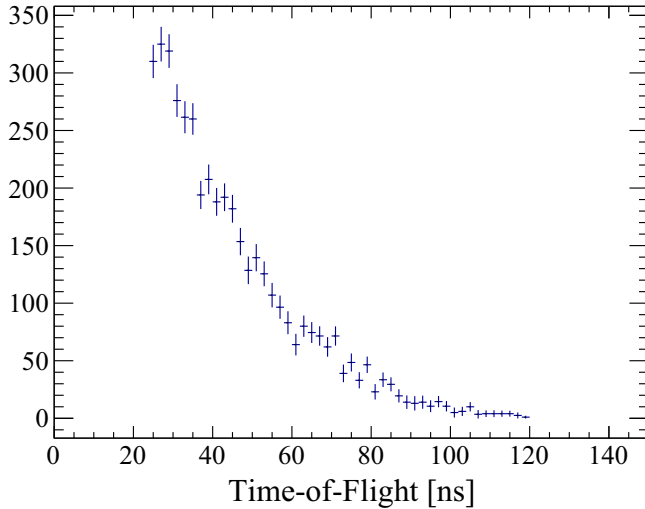


FIG. 4. Beam-induced background model from LENDA bars at angles $>66^\circ$. Both the statistical error shown and the systematic error introduced from scaling this model for each LENDA bar were propagated to the final result.

the uncertainties in the counts below $E_x = 0$ MeV for each LENDA bar were propagated to the systematic error in the final result.

Projections of the raw data and the two background models onto the excitation-energy axis are shown in Fig. 5. The background is largest at the most forward angles. However, the two peaks of interest at about 1 MeV and 3 MeV that are associated with GT transitions (discussed below) are also most prominent at forward angles, especially in the 4° – 6° angular bin, and the models clearly remove the background underneath these two peaks. This is further illustrated by the background-subtracted data shown in the laboratory frame and center-of-mass frame in Figs. 6 and 7, respectively. The remaining background in the negative-excitation-energy region averages to zero, and the data sharply increase above the $E_x = 0$ MeV kinematic line, indicating that they are representative of the charge-exchange reaction of interest.

B. Neutron-detection efficiency corrections

The measured background-subtracted counts were corrected for the neutron detection efficiency from LENDA’s geometric and intrinsic neutron-detection efficiencies plus the S800 momentum and angular acceptances using the GEANT4 simulation toolkit [49]. The neutron physics used in GEANT4 has been benchmarked with LENDA neutron-detection efficiency measurements, see Refs. [39,47].

The liquid hydrogen target was simulated as a cylinder made of liquid hydrogen with the density given in Sec. II, and a kapton foil was placed at either end of the cylinder. A ^{11}C beam with realistic position, angle, and energy spreads was simulated passing through the target. The LENDA bars were modeled as rectangular prisms made of hydrogen and carbon with a ratio of H : C = 1.104 and a density of 1.023 g/cm^3 , according to the BC-408 scintillator specifications [50]. The

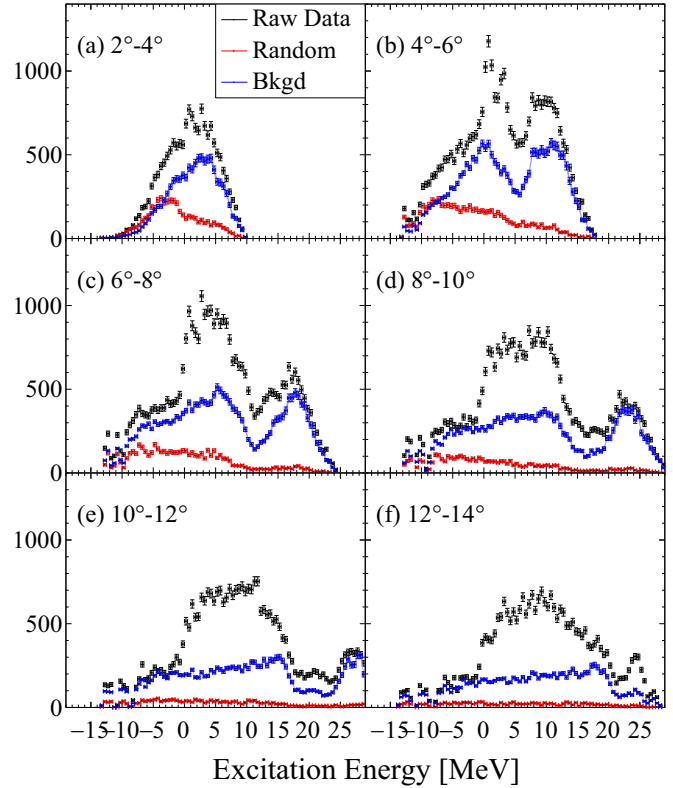


FIG. 5. Excitation-energy spectra of the raw data (black), random coincidences (red), and other background (blue). The dips in the blue background model at, e.g., 5 MeV in the 4° – 6° angular bin and 15–20 MeV in the 8° – 10° angular bin are the result of the gaps in LENDA coverage at 29.2° and 33.5° in the laboratory frame. Light blue bands (smaller than the data points on this plot) indicate systematic error in the background model.

target was placed at the origin, and the LENDA bars were placed around it according to their measured positions.

When the ^{11}C impinged on the target in the simulation, the simulation randomly selected a z position within the target as the location of the charge-exchange reaction. Upon passing

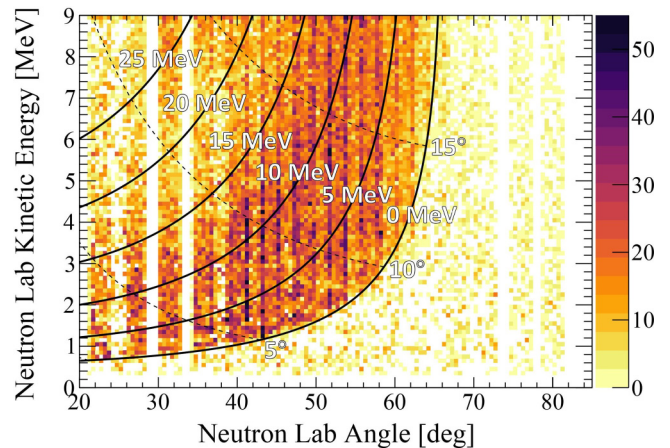


FIG. 6. Neutron laboratory energy vs. laboratory angle measured by LENDA, after background subtraction.

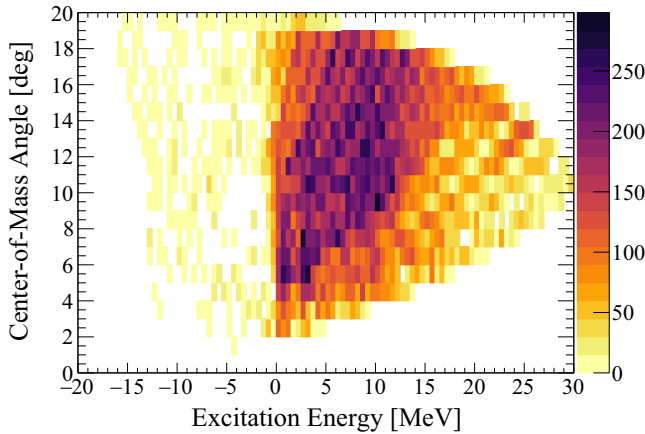


FIG. 7. Center-of-mass scattering angle vs. ^{11}N excitation energy reconstructed via a missing mass calculation, after background subtraction. Note the forward-peaking nature of the angular distribution at low excitation energies.

the selected z position, the ^{11}C was destroyed and the ^{11}N and neutron were created according to relativistic two-body kinematics. The ^{11}N was created in a state with $E_x = 0\text{--}30$ MeV at intervals of 0.1 MeV. The efficiencies were determined for each of the angular and excitation-energy bins used in the analysis of the experimental data.

The systematic error includes the error from the light-output calibration, from the measured LENDA bar positions, and from the assumptions made about the decay scheme of ^{11}N . The background-subtracted counts were divided by the efficiency to get the total number of counts. This total count was further corrected for the beam identification and reaction product identification cuts ($>99\%$), the efficiency of the S800 focal plane detectors (97%), and the data acquisition system live time (96%). Finally, the event rate was corrected for the removal of events (17%) in which multiple LENDA bars recorded hits, in part due to scattering of neutrons from one LENDA bar into another.

C. Double differential cross sections

The absolute differential cross sections were calculated from the corrected counts found in the previous section, the beam rate, and the target thickness. The resulting cross sections are shown in Fig. 8(a) for $4^\circ\text{--}6^\circ$ and Fig. 8(b) for $12^\circ\text{--}14^\circ$. The systematic errors include the uncertainty in the corrected counts discussed above, plus the uncertainties in the beam rate and target thickness (see Sec. II).

Two prominent peaks at about 1 MeV and about 3 MeV can be observed in Fig. 8(a). The height of these peaks decreases at larger angles. The forward-peaking nature of these peaks indicates that they are associated with $\Delta L = 0$ and correspond to GT transitions. Because these two states are populated by GT transitions from the ^{11}C ground state ($J^\pi = \frac{3}{2}^-$), they can be identified as the $\frac{1}{2}^-$ state at 0.73 MeV and $\frac{3}{2}^-$ state at 2.86 MeV in ^{11}N (see Table I). At higher excitation energies, the cross section is due to a combination of states associated with different angular momentum transfers.

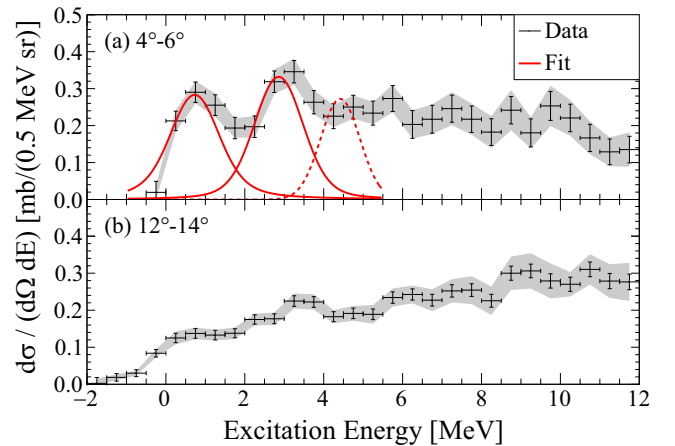


FIG. 8. Cross sections for (a) $4^\circ\text{--}6^\circ$ and (b) $12^\circ\text{--}14^\circ$. The error bars indicate the statistical error, and the gray bands indicate the systematic error. The red lines shown in (a) the $4^\circ\text{--}6^\circ$ spectrum are the fits used to extract the $B(\text{GT})$ for the first two odd-parity states. The third peak (dashed) was included to determine the background under the second peak to ensure the cross section was not overestimated.

IV. MULTIPOLE DECOMPOSITION ANALYSIS

The zero angular momentum ($\Delta L = 0$) component of the cross section must be determined before $B(\text{GT})$ can be extracted. This was done with a multipole decomposition analysis (MDA) [51,52], where the experimental cross section $\frac{d\sigma}{d\Omega}$ is fit to theoretical cross sections with $\Delta L = 0, 1, 2, \dots$:

$$\frac{d\sigma}{d\Omega} = \sum_i a_i \left(\frac{d\sigma}{d\Omega} \right)_{\text{DWBA}}^{\Delta L_i}, \quad (1)$$

where a_i are the fit parameters, and $\left(\frac{d\sigma}{d\Omega} \right)_{\text{DWBA}}^{\Delta L_i}$ are theoretical cross sections. The theoretical cross sections were calculated in the distorted wave Born approximation (DWBA) with the code DW81 [53]. The optical potential used was the global potential by Schwandt *et al.* [54] with modifications by Madland [55]. The effective nucleon-nucleon interaction used was that of Franey and Love [56]. The one-body transition densities were calculated using the code OXBASH [57] with the *wbp* interaction [58] in the *spsdpf* shell-model space.

The experimental cross sections were first smeared such that the resolution at high angles matched the resolution at low angles to minimize distortion effects that could bias the MDA. Then an MDA was done for each 0.5 MeV excitation-energy bin. In this analysis, only $\Delta L = 0$ and $\Delta L = 1$ components were used because the $\Delta L = 1$ and $\Delta L = 2$ shapes are similar in the measured angle range and using all three components

TABLE I. ENSDF adopted energies and widths used to fit the measured cross section [59].

J^π	E_x [MeV]	Γ [keV]
$\frac{1}{2}^-$	0.730(70)	600(100)
$\frac{3}{2}^-$	2.860(70)	340(40)

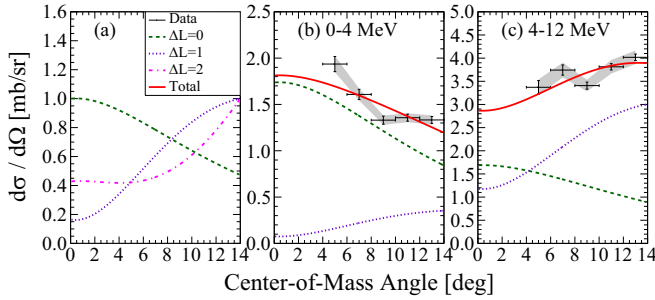


FIG. 9. (a) Angular distributions used for the MDA. The y-axis scale is arbitrary, and the curves are normalized to compare their shapes. (b) MDA for excitation energies 0–4 MeV and (c) 4–12 MeV. GT transitions ($\Delta L = 0$) dominate at excitation energies below 4 MeV, and $\Delta L > 0$ contributions grow as excitation energy increases above 4 MeV. Note that the error bars on each data point indicates the statistical uncertainties, and the grey bands indicate the systematic uncertainties.

did not reduce the uncertainties in the extracted GT strength. The transition to the first $\frac{1}{2}^+$ state in ^{11}N was used to calculate the $\Delta L = 0$ angular distribution, and the transition to the first $\frac{1}{2}^-$ state was used to calculate as the $\Delta L = 1$ angular distribution. Other transitions yielded similar angular distributions, and changing which transitions were used did not significantly affect the final extracted GT cross section. Small differences in the extracted GT cross section due to the selection of $\Delta L = 1$ or $\Delta L = 2$ angular distribution in the fit were included in the systematic uncertainties.

The angular distributions are shown in Fig. 9(a), and MDA results are shown in Fig. 9(b) for 0–4 MeV and Fig. 9(c) for 4–12 MeV. Gamow-Teller ($\Delta L = 0$) dominates below 4 MeV, and components with higher ΔL become significant at higher excitation energies. Note that the MDA took into consideration the statistical and systematic uncertainties (discussed in Sec. III B) in the extracted differential cross sections, which are indicated separately in Figs. 9(b) and 9(c). Taking into account the combined error bars, all but two data points are within one standard deviation of the fitted differential cross section, and the remaining two points are within 1.5 standard deviations, which is satisfactory. An additional component to the uncertainty is introduced by converting the extracted cross sections to Gamow-Teller strengths, as discussed in the next section.

The total $\Delta L = 0$ cross section was also extracted for the peaks at 0.73 MeV and 2.86 MeV. These peaks were fit with Voigt functions (convolution of a Lorentzian and a Gaussian distribution) to estimate the total differential cross section for each state. The MDA results discussed above were used to determine the $\Delta L = 0$ fraction of each cross section. The fit is shown in Figure 8(a) for $\theta_{\text{c.m.}} = 4^\circ - 6^\circ$. The peak energies and intrinsic (Lorentzian) widths were fixed to ENSDF adopted values, given in Table I [59]. The smearing of each peak due to the experimental resolution (Gaussian width) was fixed to the resolution determined by the GEANT4 simulation. To account for higher-lying states that may overlap with the $\frac{3}{2}^-$ peak, a third peak was included in the fit, shown as the dashed red

line in Fig. 8(a). This could, for example, be the $\frac{5}{2}^-$ state at 4.42 MeV.

V. $B(\text{GT})$ EXTRACTION

The CE cross section extrapolated to zero momentum transfer, $\frac{d\sigma}{d\Omega}(q=0)|_{\Delta L=0}$, is proportional to $B(\text{GT})$ via a proportionality constant $\hat{\sigma}_{\text{GT}}$ called the unit cross section [8]:

$$\frac{d\sigma}{d\Omega}(q=0)\Big|_{\Delta L=0} = \hat{\sigma}_{\text{GT}} B(\text{GT}). \quad (2)$$

To apply Eq. (2), the $\Delta L = 0$ cross section found in the previous section must be extrapolated to zero momentum transfer ($q = 0$), where both the scattering angle and Q value are zero. The $\Delta L = 0$ cross section at 0° can be reliably extrapolated to $Q = 0$ by using a scaling factor obtained from the DWBA calculations [8]. In this case, the scaling factor ranged from 1.3 for $E_x = 0$ MeV up to 2.0 for $E_x = 12$ MeV. The resulting $B(\text{GT})$ values are $0.18(1)^{\text{stat}}(3)^{\text{sys}}$ and $0.18(1)^{\text{stat}}(4)^{\text{sys}}$ for the $\frac{1}{2}^-$ and $\frac{3}{2}^-$ states, respectively. The cumulative $B(\text{GT})$ up to 10 MeV is $0.61(3)^{\text{stat}}(12)^{\text{sys}}$.

The unit cross section was taken from the $^{11}\text{B}(n, p)^{11}\text{Be}$ ($E_n = 96$ MeV) analysis by Ringbom *et al.* to be $\hat{\sigma}_{\text{GT}} = 8.4$ mb/sr [10]. The uncertainty in this value was estimated to be 1.0 mb/sr based on unit cross sections from β decay and CE reactions of neighboring nuclei: $^{12,13}\text{C}(n, p)$ at 95 MeV [60] and $^{10}\text{B}(n, p)$ at 96 MeV [10].

An additional uncertainty in the proportionality relationship, Eq. (2), is coherent interference of the $\Delta L = 2$, $\Delta S = 1$ component with the $\Delta L = 0$, $\Delta S = 1$ component (both are associated with $\Delta J^\pi = 1^+$). The $\Delta L = 2$, $\Delta S = 1$ component is mediated mainly by the tensor- τ component of the effective interaction, and, following Ref. [61], its effect on the cross section was estimated by switching off the tensor parts of the Franey and Love effective interaction in the DW81 program. The cross section changed by no more than 5%, which is small relative to the other systematic errors in this experiment.

Only the $^{10}\text{C}+p$ final state data have been considered so far, but ^{11}N can also decay to $2\alpha + 3p$ above $E_x \approx 2.7$ MeV. (^{11}N decays by $2p$ emission to ^9B , which decays by proton emission to ^8Be , which decays to 2α .) The direct (p, n) reaction populates proton-particle neutron-hole states in ^{11}N , and the decay by proton emission is expected to be the preferred decay channel. Nevertheless, α particles were measured in the S800 focal plane to study this alternative decay channel. No significant signal above background was observed in this channel below 4 MeV. At higher excitation energies, only an upper limit of 65% of the $^{10}\text{C}+p$ channel could be determined. However, separating the signal from the background was difficult. Given that the angular distributions of the data appeared similar to the background observed in the channel with a $^{10}\text{C}+p$ final state, the actual yield from the $2\alpha + 3p$ channel is probably much lower than this upper limit. Extracting the $\Delta L = 0$ yield from the $2\alpha + 3p$ data was not possible given the background, and this channel was excluded in the further analysis of the spectra.

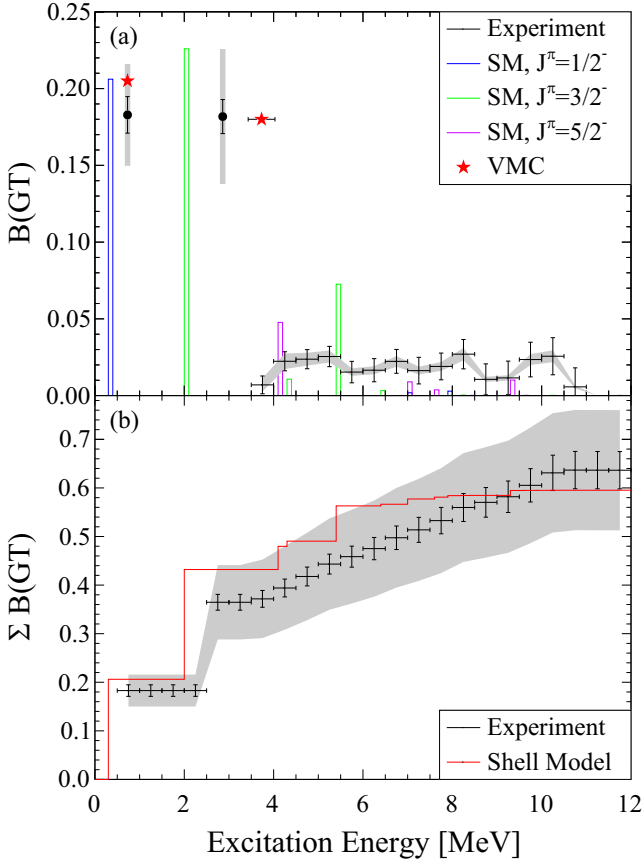


FIG. 10. (a) Comparison of the data (black, with gray bands indicating systematic error) to the shell-model calculations (blue, green, purple) and the VMC calculations (red stars). The VMC calculations did not yield excitation energies, so the energy of the $\frac{1}{2}^-$ state is fixed to the ENSDF value, and the energy of the $\frac{3}{2}^-$ state is the $\frac{1}{2}^-$ energy plus the VMC relative energy. (b) Measured cumulative $B(\text{GT})$ distribution (black, with gray bands indicating systematic error) compared to the shell-model calculation (red).

VI. DISCUSSION

The present experimental results are compared to theoretical calculations in Fig. 10, and the $B(\text{GT})$ values are presented in Table II, along with experimental results from $^{11}\text{B}(n, p)$ -

type experiments. The shell-model calculations were done in OXBASH as previously described. A scaling factor of 0.69 (Eq. (7.1) from Ref. [62]) was applied to the shell-model $B(\text{GT})$ values to account for the well-known quenching of the GT strength relative to shell-model calculations. The experimental $B(\text{GT})$ results agree with the shell-model calculations for both the individual states and for the cumulative distribution. However, as discussed above, we cannot exclude some additional GT strength to be present in the $^{11}\text{N} \rightarrow 2\alpha + 3p$ channel.

VMC calculations for both the proton- and neutron-rich cases were performed using the $NV2 + 3 - Ia^* NN$ and $3N$ interactions [63–67], following the procedure described in Ref. [67]. No additional scaling or quenching factors were applied. A VMC calculation was not done for the ground state, so excitation energies could not be calculated. The relative energy between the $\frac{1}{2}^-$ and $\frac{3}{2}^-$ states was 3.0 ± 0.3 MeV. The VMC $B(\text{GT})$ values are consistent with both the present experimental results and the shell model calculations. The VMC results are also very similar for both the $^{11}\text{C} \rightarrow ^{11}\text{N}$ and the mirror $^{11}\text{B} \rightarrow ^{11}\text{Be}$ cases, suggesting that isospin symmetry holds.

Note that the uncertainties on the VMC calculations shown in Table II are statistical as we have used only one model for this study. Based on the previous study of GT matrix elements with all available $NV2 + 3$ model classes [65], the variation due to the choice of interaction is typically 2% to 4%. Assuming a conservative 5% model uncertainty on the matrix elements would result in a 10% model uncertainty on the $B(\text{GT})$ values from VMC. Performing a Green’s function Monte Carlo (GFMC) propagation should provide a more accurate value of the $B(\text{GT})$. GFMC calculations typically quench the GT matrix element by 2% to 3% from the VMC value, which would lead to results that are still in good agreement with the data. This transition should be analyzed with GFMC in the future to confirm our expectation, and work is already underway to obtain GT matrix elements from GFMC for $A \geq 11$ with the $NV2 + 3$.

In addition to theoretical calculations, the results can also be compared to experimental $B(\text{GT})$ values obtained from mirror $^{11}\text{B}(n, p)$ -type reactions. The $^{11}\text{B}(n, p)$ reaction was measured at $E_n = 96$ MeV at the Svedberg Laboratory in Uppsala, Sweden [10]. Although the excitation energy resolution was too poor [3.5–4.5 MeV (FWHM)] to extract strengths

TABLE II. $B(\text{GT})$ comparison to theoretical calculations and to mirror (n, p)-type experiments.

	$B(\text{GT})[\frac{1}{2}^-]$	$B(\text{GT})[\frac{3}{2}^-]$	$\sum_{E_x=0}^{10 \text{ MeV}} B(\text{GT})$
$^{11}\text{C}(p, n)^a$	0.18(1) ^{stat} (3) ^{sys}	0.18(1) ^{stat} (4) ^{sys}	0.61(3) ^{stat} (12) ^{sys}
Shell model ^a	0.2061	0.2259	0.5950
VMC $^{11}\text{C} \rightarrow ^{11}\text{N}^a$	0.2050(7) ^b	0.180(1) ^b	–
VMC $^{11}\text{B} \rightarrow ^{11}\text{Be}^a$	0.2012(4) ^b	0.175(1) ^b	–
$^{11}\text{B}(n, p)$ [10]	–	–	0.75(8)
$^{11}\text{B}(d, ^2\text{He})$ [11]	$\approx 0.34^c$	$\approx 0.33^c$	–
$^{11}\text{B}(t, ^3\text{He})$ [12]	0.23(5)	0.17(5)	–

^aThis work.

^bErrors shown are statistical only. Model uncertainties contribute an additional 10% error. See text for details.

^cFrom Fig. 3(a) of Ref. [11].

for individual states, the $B(GT)$ summed to 10 MeV was 0.75(8). The $^{11}\text{B}(d, ^2\text{He})$ reaction was measured at $E_d = 270$ MeV at the RIKEN Accelerator Research Facility [11] and the $^{11}\text{B}(t, ^3\text{He})$ reaction was measured at 127 MeV/A at the NSCL [12]. Both extracted $B(GT)$ for the $\frac{1}{2}^-$ and $\frac{3}{2}^-$ states, but the $(d, ^2\text{He})$ results are significantly larger than the $(t, ^3\text{He})$ results and were consistent with the shell-model calculations without the expected quenching. The present $^{11}\text{C}(p, n)$ results are consistent with the (n, p) results and the $(t, ^3\text{He})$ results. Again, as shown in Table II, the VMC calculations predict very similar GT transition strengths for the transitions to the $\frac{1}{2}^-$ and $\frac{3}{2}^-$ states in ^{11}N and ^{11}Be .

VII. CONCLUSION

To summarize, $B(GT)$ for the transitions from $^{11}\text{C}[g.s.]$ to $^{11}\text{N}[\frac{1}{2}^-]$ and $^{11}\text{N}[\frac{3}{2}^-]$, plus the cumulative $B(GT)$ up to 10 MeV in ^{11}N , were extracted via the $^{11}\text{C}(p, n)$ reaction in inverse kinematics at 95 MeV/u. Both shell-model and *ab initio* variational Monte Carlo calculations reproduce the data well. Additionally, the results are consistent with previous (n, p) and $(t, ^3\text{He})$ $B(GT)$ measurements to the mirror states in ^{11}Be . The results indicate that the GT transitions are consistent with what is expected for p -shell nuclei. The agreement between shell-model and variational Monte Carlo calculations is also consistent with this picture. Similar to the $^{12}\text{B}(^7\text{Li}, ^7\text{Be})$ ^{12}Be study of Ref. [9] that measured the p -shell component of the first two 0^+ states in ^{12}Be , this p -shell approach is a useful complement to previous studies that probed the sd -shell components of these states, further elucidating the mixing of different configurations.

This work has demonstrated the feasibility of extracting $B(GT)$ from the (p, n) charge-exchange reaction in inverse kinematics with proton-rich rare-isotope beams. However, the experiment also indicated that future efforts, especially for proton-rich nuclei, can benefit from better ways to reduce and estimate background. The background subtraction introduces

significant systematic and statistical uncertainties and makes the extraction of GT strength from reactions that produce complex final exit channels (such as the $2\alpha + 3p$ channel in this work) very challenging. The background from γ rays could be greatly reduced by employing neutron detectors with pulse-shape discrimination capabilities, and a project to develop an array of such detectors is underway at the Facility for Rare Isotope Beams.

ACKNOWLEDGMENTS

We thank the National Superconducting Cyclotron Laboratory staff for their support. This work was supported by the US National Science Foundations No. PHY-1565546 (Operation of the NSCL), No. PHY-1913554 (Windows on the Universe: Nuclear Astrophysics at the NSCL), No. PHY-1430152 (JINA Center for the Evolution of the Elements), and No. PHY-2110365; and by the U.S. Department of Energy, Office of Nuclear Science, under Contract No. DE-SC0021027 (S.P. and G.B.K.), a 2021 Early Career Award No. DE-SC0022002 (M.P.), and Contract No. DE-AC02-06CH11357 (R.B.W.) and by the Facility for Rare Ion Beams Theory Alliance Award No. DE-SC0013617 (S.P. and M.P.) and the U.S. Department of Energy NNSA Stewardship Science Graduate Fellowship under Cooperative Agreement No. DE-NA0003960 (G.B.K.). The work of R.B.W. has been supported by the Nuclear Computational Low-Energy Initiative (NUCLEI) SciDAC project. The VMC calculations were performed using the resources of the Argonne Leadership Computing Resource Center, Argonne National Laboratory, and the computers of the Argonne Leadership Computing Facility via the 2021/2022 ALCC grant “Quantum Monte Carlo Calculations of Nuclei up to ^{16}O and Neutron Matter” for the project QMCNuc. J.C.Z. thanks the support by Fundação de Amparo a Pesquisa do Estado de São Paulo (FAPESP) under Grants No. 2018/04965-4 and 2016/17612-7.

-
- [1] I. Tanihata, Neutron halo nuclei, *J. Phys. G: Nucl. Part. Phys.* **22**, 157 (1996).
- [2] B. Jonson, Light dripline nuclei, *Phys. Rep.* **389**, 1 (2004).
- [3] I. Tanihata, H. Savajols, and R. Kanungo, Recent experimental progress in nuclear halo structure studies, *Prog. Part. Nucl. Phys.* **68**, 215 (2013).
- [4] B. Blank and M. Płoszajczak, Two-proton radioactivity, *Rep. Prog. Phys.* **71**, 046301 (2008).
- [5] M. Pfützner, M. Karny, L. V. Grigorenko, and K. Riisager, Radioactive decays at limits of nuclear stability, *Rev. Mod. Phys.* **84**, 567 (2012).
- [6] D. H. Wilkinson and D. E. Alburger, Beta decay of ^{11}Be , *Phys. Rev.* **113**, 563 (1959).
- [7] I. Talmi and I. Unna, Order of Levels in the Shell Model and Spin of ^{11}Be , *Phys. Rev. Lett.* **4**, 469 (1960).
- [8] T. N. Taddeucci, C. A. Goulding, T. A. Carey, R. C. Byrd, C. D. Goodman, C. Gaarde, J. Larsen, D. Horen, J. Rapaport, and E. Sugarbaker, The (p, n) reaction as a probe of beta decay strength, *Nucl. Phys. A* **469**, 125 (1987).
- [9] R. Meharchand, R. G. T. Zegers, B. A. Brown, S. M. Austin, T. Baugher, D. Bazin, J. Deaven, A. Gade, G. F. Grinyer, C. J. Guess *et al.*, Probing Configuration Mixing in ^{12}Be with Gamow-Teller Transition Strengths, *Phys. Rev. Lett.* **108**, 122501 (2012).
- [10] A. Ringbom, J. Blomgren, H. Condé, K. Elmgren, N. Olsson, J. Rahm, T. Rönnqvist, O. Jonsson, L. Nilsson, P. U. Renberg *et al.*, The $^{10,11}\text{B}(n, p)^{10,11}\text{Be}$ reactions at $E_n = 96$ MeV, *Nucl. Phys. A* **679**, 231 (2001).
- [11] T. Ohnishi, H. Sakai, H. Okamura, T. Niizeki, K. Itoh, T. Uesaka, Y. Satou, K. Sekiguchi, K. Yakou, S. Fukusaka *et al.*, Study of spin-isospin excitations in ^{11}Be via the $(d, ^2\text{He})$ reaction at 270 MeV, *Nucl. Phys. A* **687**, 38 (2001).
- [12] I. Daito, H. Akimune, S. M. Austin, D. Bazin, G. P. A. Berg, J. A. Brown, B. S. Davids, Y. Fujita, H. Fujimura, M. Fujiwara *et al.*, Gamow-Teller strengths from $(t, ^3\text{He})$ charge-exchange reactions on light nuclei, *Phys. Lett. B* **418**, 27 (1998).
- [13] W. Benenson, E. Kashy, D. H. Kong-A-Siou, A. Moalem, and H. Nann, $T = \frac{3}{2}$ states in mass-11 nuclei, *Phys. Rev. C* **9**, 2130 (1974).

- [14] A. Azhari, T. Baumann, J. A. Brown, M. Hellström, J. H. Kelley, R. A. Kryger, D. J. Millener, H. Madani, E. Ramakrishnan, D. E. Russ, T. Suomijarvi, M. Thoennessen, and S. Yokoyama, Proton decay of states in ^{11}N , *Phys. Rev. C* **57**, 628 (1998).
- [15] A. Lépine-Szily, J. M. Oliveira, A. N. Ostrowski, H. G. Bohlen, R. Lichtenthaler, A. Blazevic, C. Borcea, V. Guimarães, R. Kalpakchieva, V. Lapoux *et al.*, Study of excited levels of the unbound nucleus ^{11}N , *Acta Phys. Pol. B* **30**, 1441 (1999).
- [16] J. M. Oliveira, Jr., A. Lépine-Szily, H. G. Bohlen, A. N. Ostrowski, R. Lichtenthaler, A. Di Pietro, A. Laird, G. F. Lima, L. Maunoury, F. de Oliveira Santos, P. Roussel-Chomaz, H. Savajols, W. Trinder, A. C. C. Villari, and A. deVismes, Observation of the ^{11}N Ground State, *Phys. Rev. Lett.* **84**, 4056 (2000).
- [17] V. Guimarães, S. Kubono, F. C. Barker, M. Hosaka, S. C. Jeong, I. Katayama, T. Miyachi, T. Nomura, M. H. Tanaka, Y. Fuchi *et al.*, Spectroscopic study of the unbound ^{11}N nucleus, *Braz. J. Phys.* **33**, 263 (2003).
- [18] T. B. Webb, R. J. Charity, J. M. Elson, D. E. M. Hoff, C. D. Pruitt, L. G. Sobotka, K. W. Brown, J. Barney, G. Cerizza, J. Estee *et al.*, Particle decays of levels in $^{11,12}\text{N}$ and ^{12}O investigated with the invariant-mass method, *Phys. Rev. C* **100**, 024306 (2019).
- [19] L. Axelsson, M. J. G. Borge, S. Fayans, V. Z. Goldberg, S. Grévy, D. Guillemaud-Mueller, B. Jonson, K. M. Källman, T. Lönnroth, M. Lewitowicz *et al.*, Study of the unbound nucleus ^{11}N by elastic resonance scattering, *Phys. Rev. C* **54**, R1511 (1996).
- [20] K. Markenroth, L. Axelsson, S. Baxter, M. J. G. Borge, C. Donzaud, S. Fayans, H. O. U. Fynbo, V. Z. Goldberg, S. Grévy, D. Guillemaud-Mueller *et al.*, Crossing the dripline to ^{11}N using elastic resonance scattering, *Phys. Rev. C* **62**, 034308 (2000).
- [21] E. Casarejos, C. Angulo, P. J. Woods, F. C. Barker, P. Descouvemont, M. Aliotta, T. Davinson, P. Demaret, M. Gaelens, P. Leleux *et al.*, Low-lying states in the unbound ^{11}N nucleus, *Phys. Rev. C* **73**, 014319 (2006).
- [22] A. Kumar, R. Kanungo, A. Calci, P. Navrátil, A. Sanetullaev, M. Alcorta, V. Bildstein, G. Christian, B. Davids, J. Dohet-Eraly *et al.*, Nuclear Force Imprints Revealed on the Elastic Scattering of Protons with ^{10}C , *Phys. Rev. Lett.* **118**, 262502 (2017).
- [23] F. Osterfeld, Nuclear spin and isospin excitations, *Rev. Mod. Phys.* **64**, 491 (1992).
- [24] M. D. Cortina-Gil, P. Roussel-Chomaz, N. Alamanos, J. Barrette, W. Mittig, F. Auger, Y. Blumenfeld, J. M. Casandjian, M. Chartier, V. Fekou-Youmbi *et al.*, Search for the signature of a halo structure in the $p(^6\text{He}, ^6\text{Li})n$ reaction, *Phys. Lett. B* **371**, 14 (1996).
- [25] M. D. Cortina-Gil, A. Pakou, N. Alamanos, W. Mittig, P. Roussel-Chomaz, F. Auger, J. Barrette, Y. Blumenfeld, J. M. Casandjian, M. Chartier *et al.*, Charge-exchange reaction induced by ^6He and nuclear densities, *Nucl. Phys. A* **641**, 263 (1998).
- [26] J. A. Brown, D. Bazin, W. Benenson, J. Caggiano, M. Fauerbach, M. Hellström, J. H. Kelley, R. A. Kryger, R. Pfaff, B. M. Sherrill *et al.*, Measurement of the $^1\text{H}(^6\text{He}, ^6\text{Li})n$ reaction in inverse kinematics, *Phys. Rev. C* **54**, R2105 (1996).
- [27] S. Shimoura, T. Teranishi, Y. Ando, M. Hirai, N. Iwasa, T. Kikuchi, S. Moriya, T. Motobayashi, T. Murakami, T. Nakamura *et al.*, Charge exchange reaction of the neutron-halo nucleus ^{11}Li , *Nucl. Phys. A* **616**, 208 (1997).
- [28] T. Teranishi, S. Shimoura, Y. Ando, M. Hirai, N. Iwasa, T. Kikuchi, S. Moriya, T. Motobayashi, H. Murakami, T. Nakamura *et al.*, Isobaric analog state of ^{11}Li , *Phys. Lett. B* **407**, 110 (1997).
- [29] S. Shimoura, T. Teranishi, Y. Ando, M. Hirai, N. Iwasa, T. Kikuchi, S. Moriya, T. Motobayashi, T. Murakami, T. Nakamura *et al.*, Isobaric analog state of ^{11}Li , *Nucl. Phys. A* **630**, 387 (1998).
- [30] S. Takeuchi, S. Shimoura, T. Motobayashi, H. Akiyoshi, Y. Ando, N. Aoi, Z. Fü, T. Gomi, Y. Higurashi, M. Hirai *et al.*, Isobaric analog state of ^{14}Be , *Phys. Lett. B* **515**, 255 (2001).
- [31] Z. Li, W. Liu, X. Bai, Y. Wang, G. Lian, Z. Li, and S. Zeng, First observation of neutron-proton halo structure for the 3.563 MeV 0^+ state in ^6Li via $^1\text{H}(^6\text{He}, ^6\text{Li})n$ reaction, *Phys. Lett. B* **527**, 50 (2002).
- [32] Y. Satou, T. Nakamura, N. Fukuda, T. Sugimoto, Y. Kondo, N. Matsui, Y. Hashimoto, T. Nakabayashi, Y. Okumura, M. Shinohara *et al.*, Invariant mass spectroscopy of $^{19,17}\text{C}$ and ^{14}B using proton inelastic and charge-exchange reactions, *Nucl. Phys. A* **834**, 404c (2010).
- [33] Y. Satou, T. Nakamura, Y. Kondo, N. Matsui, Y. Hashimoto, T. Nakabayashi, T. Okumura, M. Shinohara, N. Fukuda, T. Sugimoto *et al.*, $^{14}\text{Be}(p, n)^{14}\text{B}$ reaction at 69 MeV in inverse kinematics, *Phys. Lett. B* **697**, 459 (2011).
- [34] M. Sasano, G. Perdikakis, R. G. T. Zegers, S. M. Austin, D. Bazin, B. A. Brown, C. Caesar, A. L. Cole, J. M. Deaven, N. Ferrante *et al.*, Gamow-Teller Transition Strengths from ^{56}Ni , *Phys. Rev. Lett.* **107**, 202501 (2011).
- [35] M. Sasano, G. Perdikakis, R. G. T. Zegers, S. M. Austin, D. Bazin, B. A. Brown, C. Caesar, A. L. Cole, J. M. Deaven, N. Ferrante *et al.*, Extraction of Gamow-Teller strength distributions from ^{56}Ni and ^{55}Co via the (p, n) reaction in inverse kinematics, *Phys. Rev. C* **86**, 034324 (2012).
- [36] J. Yasuda, M. Sasano, R. G. T. Zegers, H. Baba, W. Chao, M. Dozono, N. Fukuda, N. Inabe, T. Isobe, G. Jhang *et al.*, Inverse kinematics (p, n) reactions studies using the WINDS slow neutron detector and the SAMURAI spectrometer, *Nucl. Instrum. Methods Phys. Res. B* **376**, 393 (2016).
- [37] J. Yasuda, M. Sasano, R. G. T. Zegers, H. Baba, D. Bazin, W. Chao, M. Dozono, N. Fukuda, N. Inabe, T. Isobe *et al.*, Extraction of the Landau-Migdal Parameter from the Gamow-Teller Giant Resonance in ^{132}Sn , *Phys. Rev. Lett.* **121**, 132501 (2018).
- [38] M. Kobayashi, K. Yako, S. Shimoura, M. Dozono, N. Fukuda, N. Inabe, D. Kameda, S. Kawase, K. Kisamori, T. Kubo *et al.*, Spin-isospin response of the neutron-rich nucleus ^8He via the (p, n) reaction in inverse kinematics, in *Proceedings of the Conference on Advances in Radioactive Isotope Science (ARIS2014)* (Physical Society of Japan, Tokyo, Japan, 2015), p. 030089.
- [39] S. I. Lipschutz, The (p, n) charge-exchange reaction in inverse kinematics as a probe for isovector giant resonances in exotic nuclei, Ph.D. thesis, Michigan State University, 2018.
- [40] L. Stuhl, M. Sasano, J. Gao, Y. Hirai, K. Yako, T. Wakasa, D. S. Ahn, H. Baba, A. I. Chilug, S. Franchoo *et al.*, Study of spin-isospin responses of radioactive nuclei with the background-reduced neutron spectrometer, PANDORA, *Nucl. Instrum. Methods Phys. Res. B* **463**, 189 (2020).
- [41] C. B. Hinke, M. Böhmer, P. Boutachkov, T. Faestermann, H. Geissel, J. Gerl, R. Gernhäuser, M. Górski, A. Gottardo, H. Grawe *et al.*, Superallowed Gamow-Teller decay of the doubly magic nucleus ^{100}Sn , *Nature (London)* **486**, 341 (2012).

- [42] P. A. Závodszky, B. Arend, D. Cole, J. DeKamp, M. Doleans, G. Machicoane, F. Marti, P. Miller, J. Moskalik, W. Nurnberger *et al.*, Design, construction, and first commissioning results of superconducting source for ions at NSCL/MSU, *Rev. Sci. Instrum.* **79**, 02A302 (2008).
- [43] F. Marti, P. Miller, D. Poe, M. Steiner, J. Stetson, and X. Y. Wu, Commissioning of the coupled cyclotron system at NSCL, in *AIP Conference Proceedings* (American Institute of Physics, New York, 2001), Vol. 600, pp. 64–68.
- [44] D. J. Morrissey, B. M. Sherrill, M. Steiner, A. Stolz, and I. Wiedenhofer, Commissioning the A1900 projectile fragment separator, *Nucl. Instrum. Methods Phys. Res. B* **204**, 90 (2003).
- [45] D. Bazin, J. A. Caggiano, B. M. Sherrill, J. Yurkon, and A. Zeller, The S800 spectrograph, *Nucl. Instrum. Methods Phys. Res. B* **204**, 629 (2003).
- [46] A. Stolz, M. Behravan, M. Regmi, and B. Golding, Heteroepitaxial diamond detectors for heavy ion beam tracking, *Diam. Relat. Mater.* **15**, 807 (2006).
- [47] G. Perdikakis, M. Sasano, S. M. Austin, D. Bazin, C. Caesar, S. Cannon, J. M. Deaven, H. J. Doster, C. J. Guess, G. W. Hitt *et al.*, LENDA: A low energy neutron detector array for experiments with radioactive beams in inverse kinematics, *Nucl. Instrum. Methods Phys. Res. A* **686**, 117 (2012).
- [48] S. Lipschutz, R. G. T. Zegers, J. Hill, S. N. Liddick, S. Noji, C. J. Prokop, M. Scott, M. Solt, C. Sullivan, and J. Tompkins, Digital data acquisition for the Low Energy Neutron Detector Array (LENDa), *Nucl. Instrum. Methods Phys. Res. A* **815**, 1 (2016).
- [49] S. Agostinelli, J. Allison, K. Amako, J. Apostolakis, H. Araujo, P. Arce, M. Asai, D. Axen, S. Banerjee, G. Barrand *et al.*, GEANT4—a simulation toolkit, *Nucl. Instrum. Methods Phys. Res. A* **506**, 250 (2003).
- [50] Saint Gobain, BC-400,BC-404,BC-408,BC-412,BC-416 Premium Plastic Scintillators, <https://www.crystals.saint-gobain.com/sites/imdf.crystals.com/files/documents/bc400-404-408-412-416-data-sheet.pdf> (2021).
- [51] M. A. Moinester, A. Trudel, K. Raywood, S. Yen, B. M. Spicer, R. Abegg, W. P. Alford, N. Auerbach, A. Celler, D. Frekers *et al.*, A study of spin isovector giant resonances with the $^{208}\text{Pb}(n, p)^{208}\text{Tl}$ reaction, *Phys. Lett. B* **230**, 41 (1989).
- [52] T. Wakasa, H. Sakai, H. Okamura, H. Otsu, S. Fujita, S. Ishida, N. Sakamoto, T. Uesaka, Y. Satou, M. B. Greenfield, and K. Hatanaka, Gamow-Teller strength of ^{90}Nb in the continuum studied via multipole decomposition analysis of the $^{90}\text{Zr}(p, n)$ reaction at 295 MeV, *Phys. Rev. C* **55**, 2909 (1997).
- [53] Program DWBA70, R. Schaeffer and J. Raynal (unpublished); extended version DW81 by J. R. Comfort (unpublished).
- [54] P. Schwandt, H. O. Meyer, W. W. Jacobs, A. D. Bacher, S. E. Vigdor, M. D. Kaitchuck, and T. R. Donoghue, Analyzing power of proton-nucleus elastic scattering between 80 and 180 MeV, *Phys. Rev. C* **26**, 55 (1982).
- [55] D. G. Madland, Progress in the development of global medium-energy nucleon-nucleus optical model potentials, [arXiv:nucl-th/9702035](https://arxiv.org/abs/nucl-th/9702035).
- [56] M. A. Franey and W. G. Love, Nucleon-nucleon t-matrix interaction for scattering at intermediate energies, *Phys. Rev. C* **31**, 488 (1985).
- [57] B. A. Brown, A. Etchegoyen, W. D. M. Rae, N. S. Godwin, W. A. Richter, C. H. Zimmerman, W. Ormand, and J. S. Winfield, OXBASH, Report No. 524, MSU-NSCL (1985).
- [58] E. K. Warburton and B. A. Brown, Effective interactions for the $0p1s0d$ nuclear shell-model space, *Phys. Rev. C* **46**, 923 (1992).
- [59] J. H. Kelley, E. Kwan, J. E. Purcell, C. G. Sheu, and H. R. Weller, Energy levels of light nuclei $A = 11$, *Nucl. Phys. A* **880**, 88 (2012).
- [60] D. S. Sorenson, X. Aslanoglou, F. P. Brady, J. R. Drummond, R. C. Haight, C. R. Howell, N. S. P. King, A. Ling, P. W. Lisowski, B. K. Park *et al.*, Energy dependence of the Gamow-Teller strength in p-shell nuclei observed in the (n, p) reaction, *Phys. Rev. C* **45**, R500 (1992).
- [61] R. G. T. Zegers, H. Akimune, S. M. Austin, D. Bazin, A. M. van den Berg, G. P. A. Berg, B. A. Brown, J. Brown, A. L. Cole, I. Daito, Y. Fujita, M. Fujiwara, S. Gales, M. N. Harakeh, H. Hashimoto, R. Hayami, G. W. Hitt, M. E. Howard, M. Itoh, J. Janecke, T. Kawabata, K. Kawase, M. Kinoshita, T. Nakamura, K. Nakanishi, S. Nakayama, S. Okumura, W. A. Richter, D. A. Roberts, B. M. Sherrill, Y. Shimbara, M. Steiner, M. Uchida, H. Ueno, T. Yamagata, and M. Yosoi, The $(t, ^3\text{He})$ and $(^3\text{He}, t)$ reactions as probes of Gamow-Teller strength, *Phys. Rev. C* **74**, 024309 (2006).
- [62] W. T. Chou, E. K. Warburton, and B. A. Brown, Gamow-Teller beta-decay rates for $A \leq 18$ nuclei, *Phys. Rev. C* **47**, 163 (1993).
- [63] M. Piarulli, L. Girlanda, R. Schiavilla, R. N. Pérez, J. E. Amaro, and E. R. Arriola, Minimally nonlocal nucleon-nucleon potentials with chiral two-pion exchange including Δ resonances, *Phys. Rev. C* **91**, 024003 (2015).
- [64] M. Piarulli, L. Girlanda, R. Schiavilla, A. Kievsky, A. Lovato, L. E. Marcucci, S. C. Pieper, M. Viviani, and R. B. Wiringa, Local chiral potentials with Δ -intermediate states and the structure of light nuclei, *Phys. Rev. C* **94**, 054007 (2016).
- [65] A. Baroni, L. Girlanda, A. Kievsky, L. E. Marcucci, R. Schiavilla, and M. Viviani, Tritium β decay in chiral effective field theory, *Phys. Rev. C* **94**, 024003 (2016); **95**, 059902(E) (2017).
- [66] A. Baroni, R. Schiavilla, L. E. Marcucci, L. Girlanda, A. Kievsky, A. Lovato, S. Pastore, M. Piarulli, S. C. Pieper, M. Viviani *et al.*, Local chiral interactions, the tritium Gamow-Teller matrix element, and the three-nucleon contact term, *Phys. Rev. C* **98**, 044003 (2018).
- [67] G. B. King, L. Andreoli, S. Pastore, M. Piarulli, R. Schiavilla, R. B. Wiringa, J. Carlson, and S. Gandolfi, Chiral effective field theory calculations of weak transitions in light nuclei, *Phys. Rev. C* **102**, 025501 (2020).